

A numerical investigation of static resistance of welded planar steel tubular joints under in-plane and out-of-plane bending at elevated temperatures



E. Ozyurt^{a,b}, Y.C. Wang^{b,*}

^a Department of Civil Engineering, Gumushane University, Gumushane, Turkey

^b School of Mechanical, Aerospace and Civil Engineering, University of Manchester, UK

ARTICLE INFO

Keywords:

Circular Hollow Section (CHS)
Elevated temperature
Elliptical Hollow Section (EHS)
Joint resistance
Square Hollow Section (SHS)
T-joint
Y-joint
X-joint

ABSTRACT

This study presents the results of a numerical investigation on static resistance of welded planar steel tubular joints under in-plane and out-of-plane bending moments at elevated temperatures. The numerical simulations were carried out using the commercial finite Element software ABAQUS v6.14-1 and the simulation model was validated by comparing against test results for CHS joints under brace in-plane bending at elevated temperatures.

Extensive numerical parametric simulations were performed for CHS/SHS/EHS joints under in-plane and out-of-plane bending at elevated temperatures, to establish a database of results covering a wide range of geometrical parameters, including brace to chord diameter ratio, the angle between brace to chord members, and chord diameter to twice chord thickness ratio.

The ratios of joint elevated temperature resistance to ambient temperature resistance were compared to the steel yield strength reduction factor, the steel Young's modulus reduction factor, and the average of the above these reduction factors at different elevated temperatures. Based on the comparisons, it has been found that using the reduction factor for the yield strength of steel to modify the ambient temperature equations will overestimate the resistance of joints at elevated temperatures. As a simplified and safe recommendation, the ambient temperature joint resistance equations can be modified by the average reduction factors for the Young's modulus and yield strength at elevated temperatures. This modification factor can be increased to the yield strength reduction factor when the brace and chord widths/diameters are the same.

1. Introduction

Welded steel tubular structures are widely used in building construction for which fire safety is an important safety consideration. For this type of structures, many research studies have been devoted to understanding how welded joints behave at ambient temperature, resulting in well-established and widely accepted design equations to calculate their resistances at ambient temperature. However, investigations of welded steel tubular joint behaviour and resistance at elevated temperatures lack behind and only a limited number of studies exist. Welded steel tubular joints can have many types (e.g. T, X, Y, K, etc.), be constructed of members of different shapes (Circular Hollow Section (CHS), Square/Rectangular Hollow Section (SHS/RHS) and Elliptical Hollow Section (EHS)), and the brace members can be subjected to axial load (tension/compression), or bending moments (in-plane bending/out-of-plane bending).

With such a large array of factors to consider and the behaviour of

joints at elevated temperatures being complex, it would not be possible to repeat the extensive research efforts devoted to studies at ambient temperature. An efficient way is to make use of joint resistance calculation equations at ambient temperature and then modify them to take account of elevated temperature effects. An analysis of the failure modes of welded tubular joints is necessary to identify the most appropriate modification.

When a welded tubular joint is under axial load or in-plane bending moment or out-of-plane bending moment in the brace, the following failure modes may occur [4]; chord plastification, chord punching shear, chord side wall failure, chord shear and local yielding of the brace.

Among the above five identified failure modes, punching of the chord, local yielding of the brace and chord shear are failure modes governed by material strength (yield strength of steel). Therefore, for these three failure modes, the elevated temperature load carrying capacity of the joint can be calculated by multiplying the ambient

* Corresponding author.

E-mail address: yong.wang@manchester.ac.uk (Y.C. Wang).

Notations

The following symbols are used in this paper:

E	young's modulus	$h_{1,2}$	external depth of brace member
L	length of chord member	$k_{y,\theta}$	reduction factor for yield strength of steel at elevated temperature
M_θ	bending moment resistance in the brace member at elevated temperature	$k_{E,\theta}$	reduction factor for Young's modulus at elevated temperature
M_{20}	bending moment resistance in the brace member at ambient temperature	l	length of brace member
b_o	external width of chord member	t_o	wall thickness of chord
$b_{1,2}$	external width of brace member	$t_{1,2}$	wall thickness of brace
d_o	diameter of chord member	β	diameter ratio ($=b_1/b_o$)
$d_{1,2}$	diameter of brace member	θ	brace-to-chord intersection angle
f_y	yield stress of chord member	γ	half width to thickness ratio of the chord ($=b_o/2t_o$)
h_o	external depth of chord member	ε_T	true strain
		ε	engineering strain
		σ_T	true stress
		σ	engineering stress

temperature resistance by the steel yield strength modification factor at elevated temperatures. For chord side wall failure which involves buckling and yielding, it is possible to replace the ambient temperature material properties by those at elevated temperatures to calculate the elevated temperature resistance.

The situation for the failure mode of chord plastification is different and deserves special consideration. The load carrying capacity for chord plastification is based on bending resistance of the chord face connected to the brace member, without instability effect. This chord face is in compression (due to global bending of the chord) when the brace member is under compression and in tension when the brace member is under tension. When the chord face is in compression, and when the chord face undergoes large deformations at high temperatures, high local second-order effects exist. Therefore, depending on the relative change of strength and stiffness of steel at elevated temperatures, it may not be appropriate to calculate the elevated temperature resistance of the joint by multiplying the ambient temperature solution by the steel yield strength reduction factor.

At elevated temperatures, the yield strength of normal strength steel has higher reduction factors than the Young's modulus of steel. Since the second order effect in chord face under compression is caused by large chord face deformation, reductions in joint resistance when the brace member is under compression follow more closely to reductions in the Young's modulus of steel. This conclusion was first reached by Ozyurt et al. [20] for CHS and SHS/RHS joints, and subsequently confirmed by a number of researchers [22,23,15,16,13] for CHS/SHS/RHS joints, and by Ozyurt and Wang [19] for EHS joints when the brace members are connected to the wider face.

For all joints under brace member tension load, there is no chord face second order effect. Therefore, the joint resistance can be obtained by modifying the joint resistance at ambient temperature by the steel yield strength reduction factor at elevated temperatures.

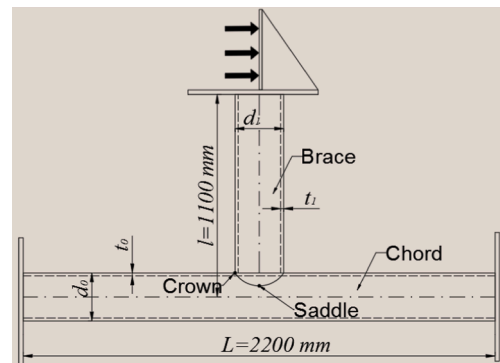
In contrast to welded steel tubular joints under brace axial load, there are very few studies of welded tubular joints under in-plane or out-of-plane bending in brace members. Nguyen et al. [18] tested five CHS T-joints under in-plane bending moment at elevated temperatures to investigate the effects of brace to chord diameter ratio on joint resistance. They found that the joint resistance at 700 °C was 0.19 that at ambient temperature, lower than the steel yield strength reduction factor of 0.26, but close to the average of steel yield strength and Young's modulus reduction factors of 0.195, according to their elevated temperature mechanical test results. Garifullin et al. [12] focused on initial rotational stiffness of welded RHS T-joints under brace in-plane bending with axial force in the chord member at ambient temperature. Some researchers have investigated the behaviour of reinforced tubular joints under bending moments, but they were limited to ambient temperature, including Chen et al. [7] who experimentally investigated

reinforced SHS X-joints subjected to the in-plane bending moment at ambient temperature, Chen and Chen [8] who introduced a design method to calculate in-plane bending moment resistance of reinforced SHS X-joints and Nassiraei et al. [17] who performed a parametric study to examine the effects of reinforcing plates on bending moment capacity of T- and Y-joints.

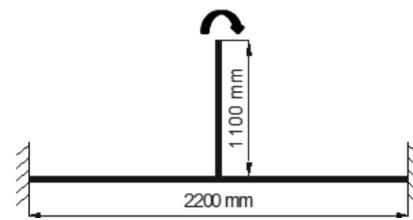
This study will investigate whether similar simplified design recommendations, as for welded tubular joints with brace axial force, can be obtained for welded tubular joints with a brace member under in-plane or out-of-plane bending moment at elevated temperatures.

2. Validation of finite element model

The results of this study are based on numerical simulations using the general finite element package ABAQUS/Standard v6.14-1 [1]. For validation, numerical simulation results are compared with any relevant tests which include those of Nguyen et al. [18] for CHS joints under in-plane bending at elevated temperatures, the ambient



a) Test arrangement



b) A numerical model with boundary conditions

Fig. 1. Typical in-plane bending test arrangement, IB.T.069 of Nguyen et al. [18].

Table 1
Dimensions of the Nguyen et al. [18] joint test specimens used for validation.

Joint Name	d_0 (mm)	d_1 (mm)	t_0 (mm)	t_1 (mm)	β (d/D)	θ (°)
IB.T.069.20 [18]	244.5 (L = 2200)	168.3 (l = 1100)	6.3	6.3	0.69	90
IB.T.069.550 [18]	244.5 (L = 2183.5)	168.3 (l = 1100)	6.3	6.3	0.69	90
IB.T.069.700 [18]	244.5 (L = 2177.9)	168.3 (l = 1100)	6.3	6.3	0.69	90

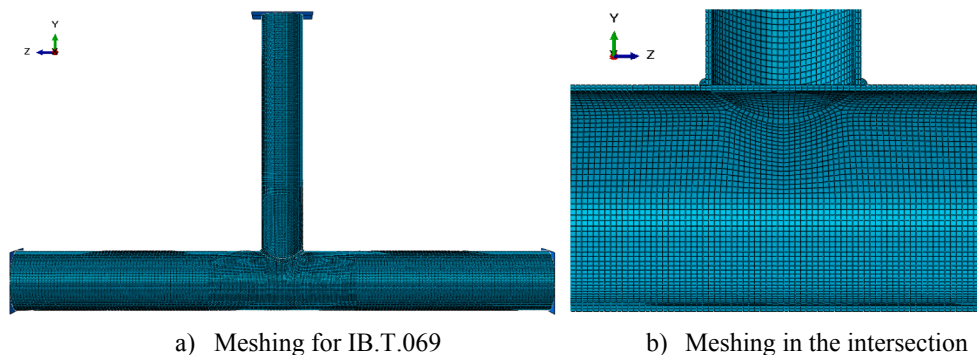


Fig. 2. Finite element mesh for test joints of Nguyen et al. [18].

Table 2
Measured mechanical properties for the test joints of Nguyen et al. [18].

Member Type	Test temperature (°C)	Young's modulus (GPa)	Yield stress (MPa)	Tensile Stress (MPa)
Brace & Chord	27.4	201.2	380.3	519.1
Brace & Chord	526.7	111.2	270.0	331.3
Brace & Chord	680.3	26.2	99.5	102.2

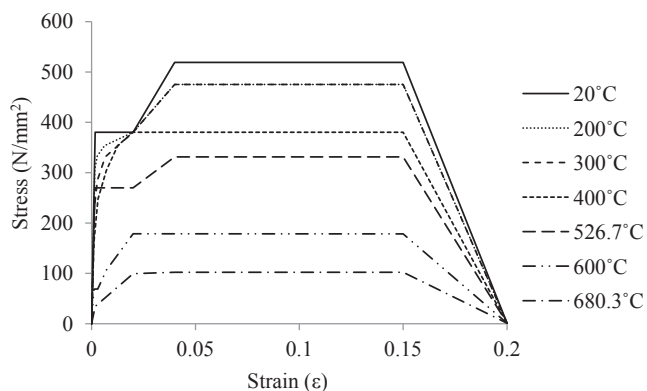


Fig. 3. Stress-strain curves of steel in the numerical model for validation study against the test results of Nguyen et al. [18].

temperature tests of Wang et al. [25] for SHS X-joints under out-of-plane bending and the fire tests of Gao et al. [11] on CHS T-joints with brace axial load. There is no available elevated temperature test on welded tubular joints with brace member under out-of-plane bending.

2.1. Comparison against test results of Nguyen et al. [18]

Nguyen et al. [18] carried out five tests of welded CHS T-joints under brace in-plane bending moment at elevated temperatures. Fig. 1(a) shows the in-plane bending test arrangement of Nguyen et al. [18]. Table 1 provides the joint dimensions for the three tests modelled by the authors. Nguyen et al. [18] did not provide temperature data for the other two tests hence they were not used in this research.

To reduce computational time, only half of the T-joint was modelled to take advantage of symmetry in geometry and loading by applying appropriate boundary conditions for symmetry. Fig. 1(b) shows the

boundary conditions used in the tests and also in the numerical simulation model.

In the ABAQUS simulation model, 20-noded solid quadratic (C3D20R) elements with reduced integration, with two elements in the thickness direction, were used for both the chord and brace members; quadratic wedge solid elements (C3D15) were used for welds for accurate meshing. The ABAQUS sweep function was used to model weld geometry. The weld geometry can be formed by using either shell elements or solid elements. Using three-dimensional solid elements allows the weld geometry to be faithfully recreated so they were used in the authors' simulation models. The brace and chord members were tied to the weld elements by using the tie function in ABAQUS with surface to surface contact. The surfaces of the brace and chord members in contact with the weld geometry were chosen as the master surface and the surface of the weld geometry was the slave surface. Fig. 2(a) and (b) show a typical finite element mesh. The same technique was previously successfully used by the authors [20] for such joints under brace axial load.

The elevated temperature tests of Nguyen et al. [18] were carried out under the steady state condition in which the temperature of the structure was raised to the required level in an electrical heating box and the mechanical load was then applied. Because of this, the Riks method was chosen to simulate the large deformation behaviour. The tests were carried out at 20 °C, 550 °C, and 700 °C.

Table 2 lists the measured ambient and elevated temperature mechanical properties of steel for the Nguyen et al. [18] tests. Fig. 3 presents the stress-strain curves of the steel material at elevated temperatures, derived from Eurocode EN-1993-1-2 [5]. In the ABAQUS simulation model, the true stress-strain curve was input after converting the engineering stress-strain curve into the true stress and logarithmic strain curve [2].

$$\varepsilon_T = \ln(1 + \varepsilon) \quad (1)$$

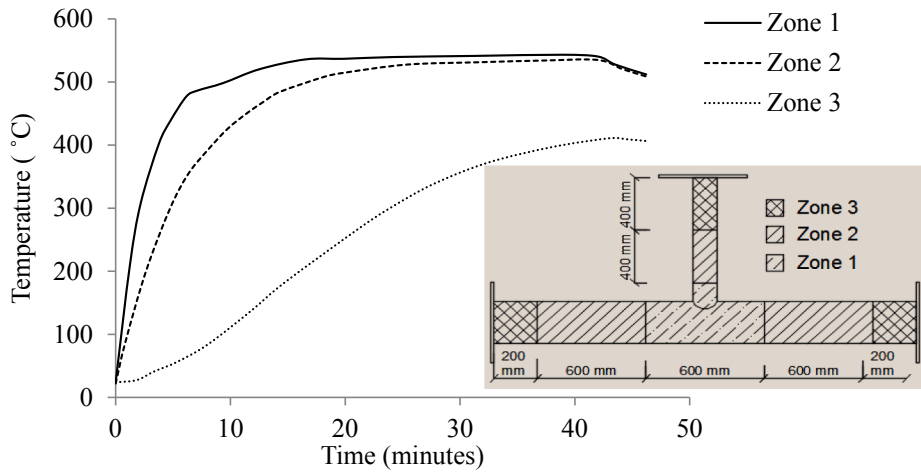


Fig. 4. Recorded temperature distributions of IB.T.069 [18] for a target temperature of 550 °C.

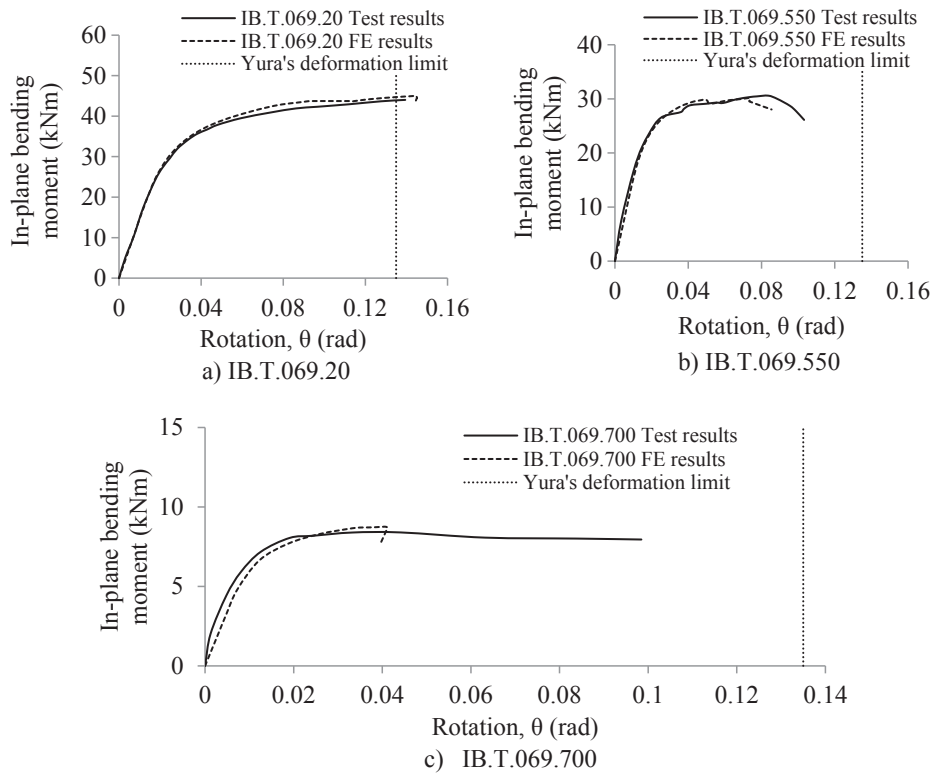


Fig. 5. Comparison of in-plane bending moment-rotation curves of IB.T.069 [18].

Table 3
Dimensions of the Wang et al. [25] joint test specimens.

Joint Name	b_o and h_o (mm)	b_l and h_l (mm)	t_o (mm)	t_l (mm)	β (b_l/b_o)	θ (°)
OPN08	150 ($L = 800$)	80 ($l = 425$)	6	5	0.53	90
OPN10	150 ($L = 800$)	100 ($l = 425$)	6	5	0.67	90
OPN12	150 ($L = 800$)	120 ($l = 425$)	6	5	0.80	90

$$\sigma_T = \sigma(1 + \epsilon)$$

(2)

where

- ϵ_T , is true strain
- ϵ , is engineering strain
- σ_T , is true stress
- σ , is engineering stress

Fig. 4 shows the recorded test temperature distribution for a target temperature of 550 °C. The joint model was partitioned into the same three zones as for measuring temperature distributions in the tests. Each zone was assumed to have uniform temperature. The three sets of measured temperature-time relationships were input for the three corresponding zones.

Nguyen et al. [18] reported in-plane bending moment-rotation

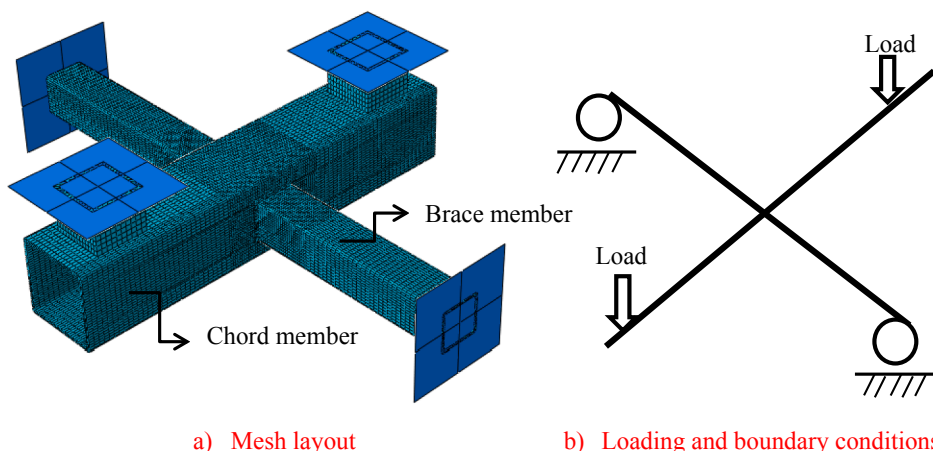


Fig. 6. Mesh layout and boundary and loading conditions of SHS X-joint (OPN08) of Wang et al. [25].

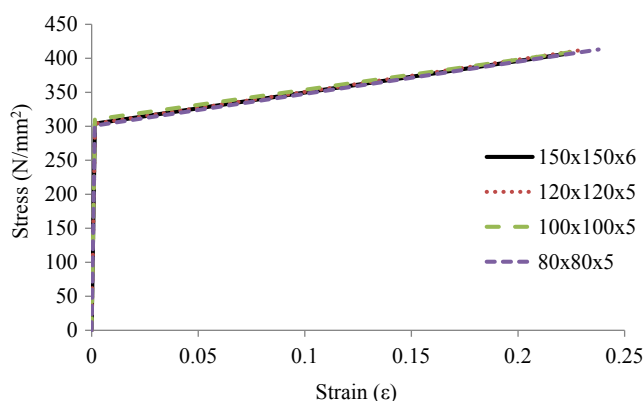


Fig. 7. Bilinear stress-strain curves of steel used in the numerical models for the tests of Wang et al. [25].

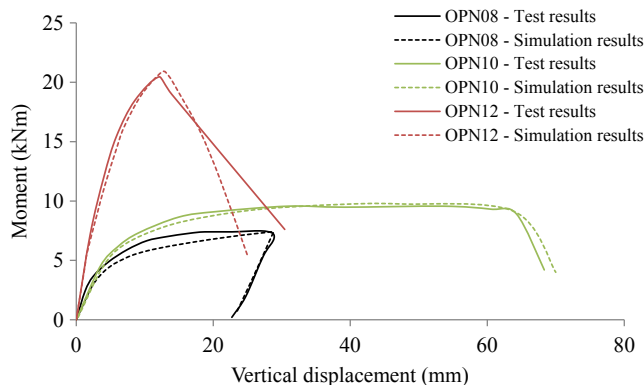


Fig. 8. Comparison of moment-vertical displacement curves between the test results of Wang et al. [25] and the authors' simulation results.

curves and Fig. 5 compares the simulation and test results. The agreement between the numerical results and the test results is very good at different elevated temperatures.

2.2. Comparison against test results of Wang et al. [25]

There was not any available test result of welded tubular joints under brace out-of-plane bending moment at elevated temperatures. However, the authors used the test results of Nguyen et al. [18] to validate the numerical model for CHS T-joints under brace in-plane bending moment at elevated temperatures. In addition, the test results

of Wang et al. [25] were used to validate the authors' simulation model for SHS X-joints under out-of-plane bending moment at ambient temperatures. Taken together, it may be accepted that the authors' numerical model is able to simulate the behaviour of welded tubular joints under out-of-plane bending moment at elevated temperatures.

Wang et al. [25] carried out 13 tests of unreinforced and reinforced SHS X-joints under brace out-of-plane bending moment at ambient temperature. The three unreinforced specimens of Wang et al. [25] were used for validation purpose of this paper. Table 3 summarises the dimensions of the Wang et al. [25] joint test specimens. The same modelling strategy as that for CHS T-joints under in-plane bending moment, in terms of element type, mesh density, weld and loading, was adopted. Fig. 6 illustrates a typical mesh layout for SHS X-joints under out-of-plane bending load. In the test, the axial load was applied to the chord member at the end of the steel stub column welded to the chord face to produce an out-of-plane bending in the joint, and the specimen was mounted on the testing ring using two supporting plates at the ends of the brace members.

Fig. 7 illustrates the bilinear stress-strain curves for the steel members based on the tensile coupon test results of Wang et al. [25].

Fig. 8 compares the simulated and measured moment-vertical displacement curves for the three tests and Fig. 9 compares the deformed shapes of one of the tests (OPN08). Both sets of results show good agreement between the test results and the authors' simulation results.

2.3. Comparison against test results of Gao et al. [11]

Gao et al. [11] carried out elevated temperature tests on reinforced and unreinforced CHS T-joints. Only the unreinforced joint was modelled due to its relevance to this paper. Fig. 10 shows the test setup. Table 4 lists the joint dimensions. The steel grade was S355 with a yield strength of 385 N/mm², an ultimate strength of 507 N/mm² and elastic modulus of 198 GPa at ambient temperature from their coupon test results. The elevated temperature stress-strain curves were based on Eurocode EN-1993-1-2 and are shown in Fig. 11.

The elevated temperature test was carried out under transient state testing condition. Heating of the specimen was provided by an electric heating furnace and Fig. 12 shows the measured furnace temperature-time relationship. Steel joint temperatures were measured at four locations as shown in Fig. 13.

A sequentially coupled thermal-stress analysis was used in this study. 20-noded solid quadratic (DC3D20) elements, with two elements in the thickness direction, were used for both the chord and brace members in both thermal and stress analyses. Fig. 14 shows a typical finite element mesh, including thermal boundary condition. For heat transfer modelling, the convective and radiation heat transfer coefficients were 25 W/(m² K) and 0.5, respectively, according to EN-1993-1-

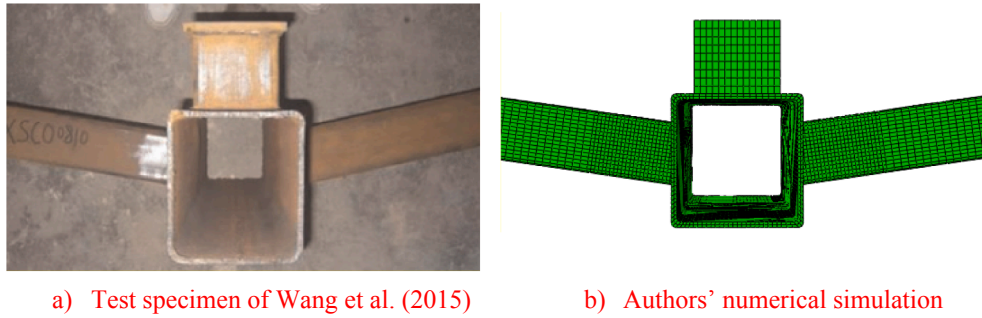


Fig. 9. Comparison of test and simulation results for the deformed shapes of OPN08 joint.

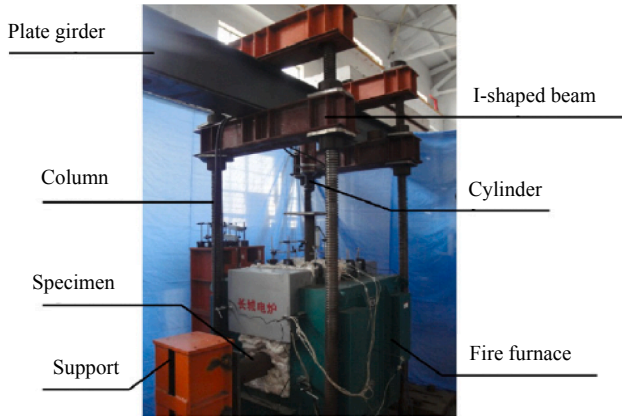


Fig. 10. Test setup of Gao et al. [11].

1 [6]. In the stress analysis, the elevated material properties of steel were based on the Eurocode 3 EN-1993-1-2 [5]. The thermal properties of steel (density, thermal conductivity, specific heat) were also in accordance with Eurocode 3 EN-1993-1-2 [5].

Fig. 15 compares the recorded and simulated temperature-time curves at the various locations, showing excellent agreement.

After heat transfer modelling, stress analysis was performed. The test results reported joint local displacement – time curve at the intersection area, and Fig. 16 compares the authors' numerical simulation and the test results of Gao et al. [11]. The test and simulation results are close.

In summary, the sequentially coupled thermal-stress analysis model can be used to analyse fire behaviour of welded tubular joints.

3. Parametric study and results

3.1. Simulation parameters

A large number of joint types were simulated, as shown in Fig. 17, consisting of T-, Y-, K- and X-joints made of CHS, SHS or EHS. In the case of EHS joints, four different orientations according to Choo et al. [10] were considered, namely type 1, 2, 3 and 4 as shown in Fig. 18.

For each joint type, different joint geometric dimensions were considered. Fig. 19 illustrates geometries of tubular joints and Tables 5, 6 and 7 summarise the geometric parameters and dimensions of the simulated CHS, SHS and EHS T-, Y-, K- and X-joints respectively. For identification, the first letter (C, E or S) represents the tubular cross-

Table 4
Dimensions of the Gao et al. [11] joint test specimens.

Joint Name	d_o (mm)	d_t (mm)	t_o (mm)	t_t (mm)	β (d_t/d_o)	θ (°)
SP1 [11]	159 ($L = 2000$)	89 ($l = 1000$)	5	4	0.56	90

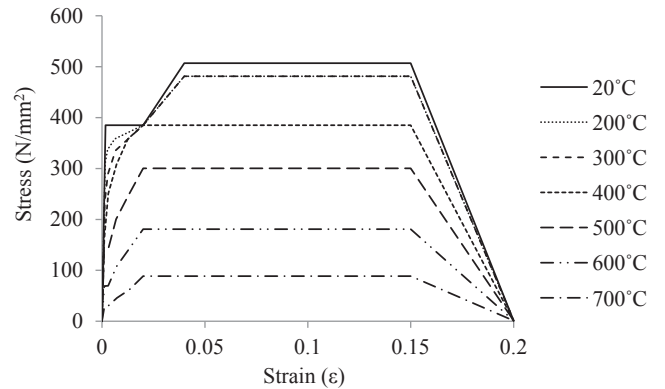


Fig. 11. Stress-strain curves of steel in the numerical model for validation study against the test results of Gao et al. [11].

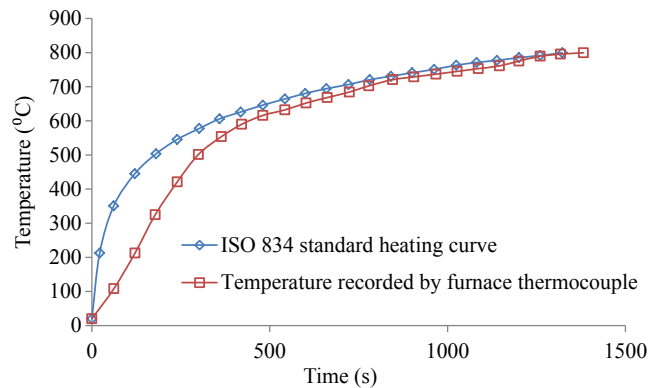


Fig. 12. Comparison of the measured temperature-time curve of Gao et al. [11] with ISO 834.

section shape (CHS, EHS or SHS), the second letter refers to the joint type (T-, Y-, K- or X-joint), the number following is the angle between the brace and the chord member and the last number is the joint number for different joint dimensions in the respective tables. The joint dimensions cover three different values of brace to chord diameter ratio β and different values of chord half width to thickness ratio. For EHS joints, the last number refers to joint type according to Fig. 18.

The joint dimensions were selected according to the range of validity of CIDECT guide No. 1 and 3 [26,21] and EN 1993-1-8 [4]. Van der Vegte et al. [24] recommended using a chord length of at least

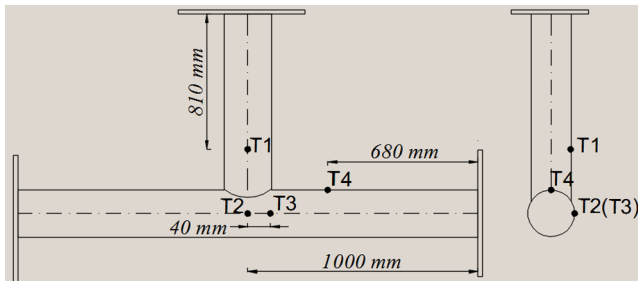


Fig. 13. Location of thermocouples on the joint in the test of Gao et al. [11].

$10d_0$ (or b_0) in order to eliminate the effects of chord end conditions and chord length effects on the behaviour and resistance of CHS T-joints. This is higher than six times as suggested by others [13,14,9]. Therefore, the chord diameter d_0 and length l_0 for all CHS joints were 244.5 mm and 2500 mm respectively. In the case of SHS and EHS joints, the chord length was determined similarly as for CHS joints. The numerical parametric study covered the range of steel temperature up to 700 °C which is the upper bound of steel temperatures at failure under realistic loading conditions. Each joint was analysed for the following five temperature levels: 20 °C, 400 °C, 500 °C, 600 °C, and 700 °C.

In all cases, the output of the simulation is joint resistance because this is the focus of fire resistance design.

In all numerical models for the parametric study, the yield strength and Young’s modulus of the brace and chord members at ambient temperatures were 355 MPa and 210 GPa, respectively. The stress-strain curves of steel at elevated temperatures were constructed according to EN-1993-1-2 [5] and they are shown in Fig. 20. The same properties of the members were used for the weld. Similar to the validation study, the engineering stress-strain curves were converted to the true stress-strain curves in the parametric study.

3.2. Effects of temperature distribution on joint resistance

When an unprotected welded tubular joint is exposed to fire, the weld is expected to attain lower temperatures than in other regions of the joint due to higher thickness of the weld. However, since the failure mode under consideration is chord face plastification, it is expected that the joint behaviour is not affected by the weld temperature being slightly lower than the chord face temperature. To confirm this, a comparison has been made for joint resistance between uniform and non-uniform temperature distributions for two exemplar cases of CT90-1 and CK45-1. Heat transfer analyses were carried out to obtain joint temperatures as previously described. The outer surfaces of the joint members were exposed to a fire whose temperature-time curve

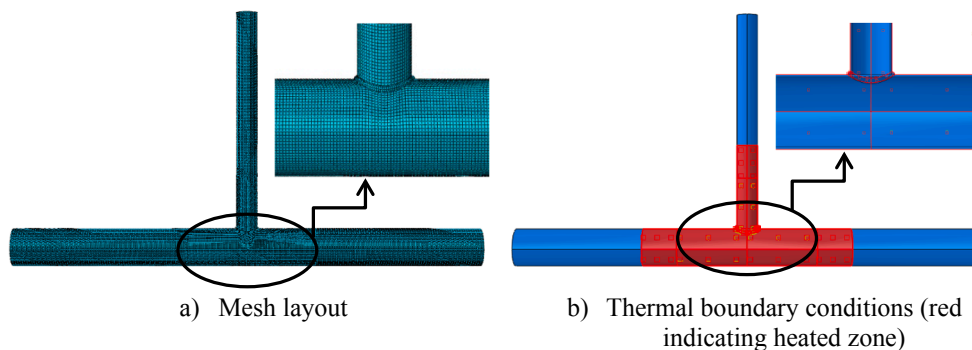


Fig. 14. Mesh layout and thermal boundary condition of FE model.

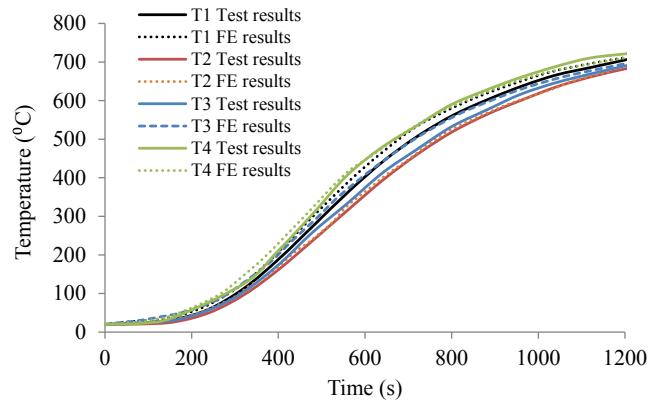


Fig. 15. Comparison of temperature – time curves between numerical simulation and test results of Gao et al. [11].

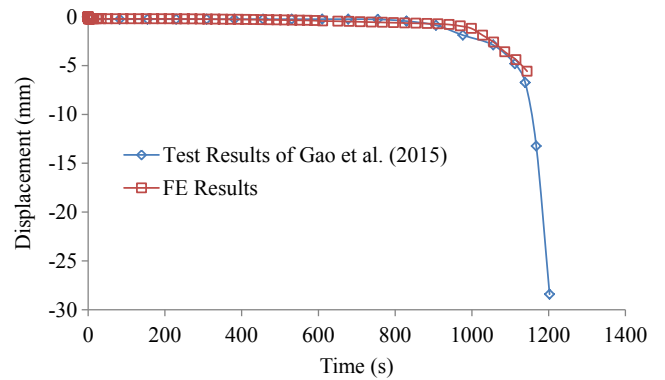


Fig. 16. Comparison of local displacement at the intersection area between the authors’ simulation results and the test results of Gao et al. [11].

followed that of Gao et al. [11]. The target chord face temperature was 700 °C, therefore the heat transfer analysis was stopped when this target temperature was reached. In the subsequent stress analysis, the brace member(s) were under either in-plane or out-plane bending moments.

Fig. 21 compares weld and chord face temperature-time curves for the two exemplar joints. At the target chord face temperature of 700 °C, the weld temperatures were much lower, at 622 °C and 612 °C for joints CT90-1 and CK45-1 respectively.

However, despite the noticeable temperature differences between at the weld and in the chord face, the joints behaved almost identically as the joints with uniform temperature distribution, as demonstrated in

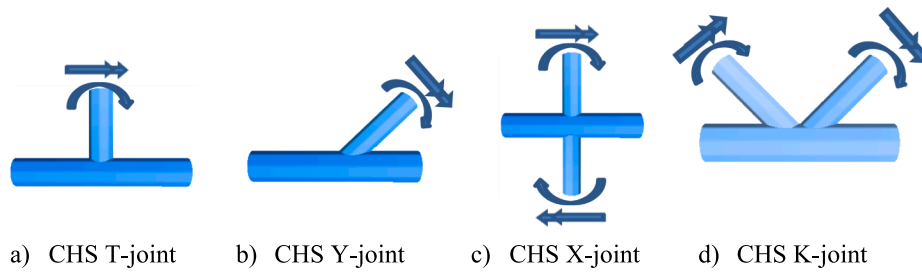


Fig. 17. Types of joints investigated.

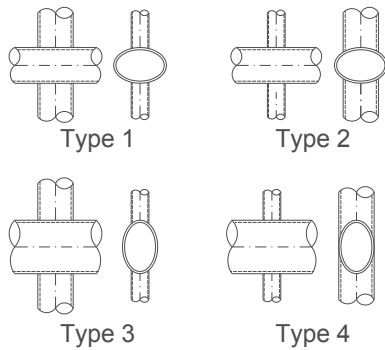
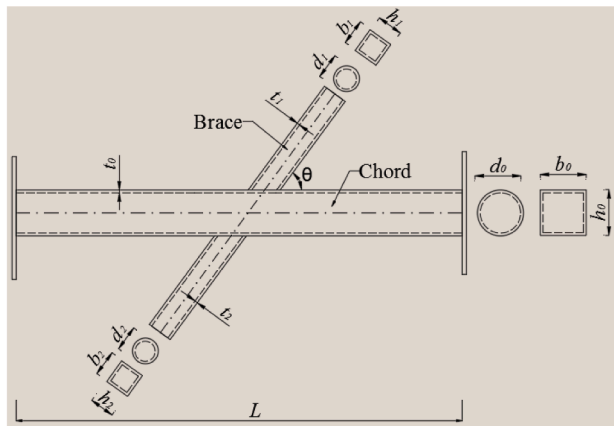
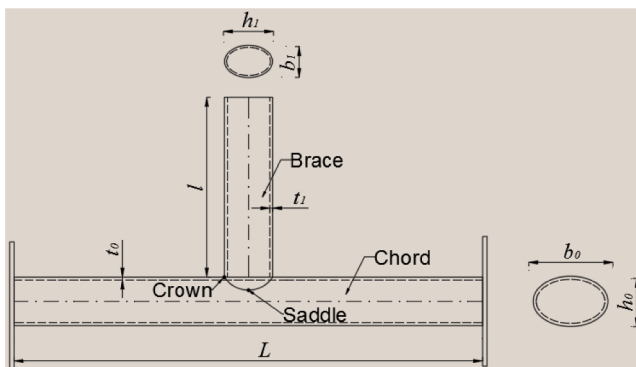


Fig. 18. EHS Joint orientations [10].



a) Tubular X-joint



b) EHS T-joint

Fig. 19. Geometries of tubular joints.

Fig. 23 for their deformation and failure modes, and in Fig. 22 for their bending moment-rotation curves and joint resistances.

3.3. Welded tubular joints under brace in-plane bending moment

3.3.1. CHS joints

Fig. 24(a) and (b) present simulation results for CHS T-, Y-, K- and X-joints, in terms of joint resistance, normalised to the ambient temperature resistance, as a function of temperature, respectively. Yura's deformation limit ($80F_y/E = 0.135 \text{ rad}$) [27] was adopted to define joint resistance at both ambient and elevated temperatures. In general, the joint resistance was equal to the peak load if the peak load occurred before reaching the deformation limit of Yura et al. [27], or equal to the load at the deformation limit if the peak load occurred after the deformation limit. As shown in Fig. 25, there is no clear appearance of the peak load at both ambient and elevated temperatures before reaching the deformation limit. Therefore, the joint resistance was determined as the value of the load at the deformation limit of Yura et al. [27]. Included in Fig. 24(a) and (b) are three curves representing steel yield strength reduction factor – temperature relationship, steel Young's modulus reduction factor – temperature relationship, and the average of the above two reduction factors – temperature relationship.

All the results in Fig. 24 indicate that the simulation results of joint resistance ratio at elevated temperatures fall between the steel Young's modulus reduction factor and the steel yield strength reduction factor and are close to the average of these two reduction factors. This can be explained by the stress behaviour of two typical joints, CT90-1 and CK45-1, in the direction of the chord member, as shown in Fig. 26(a) and (b) respectively. When the brace member is subjected to in-plane bending, half of the chord face is under a tension load and the other half of the chord face under a compression load. Hence, the reduction factor for welded tubular joints with in-plane bending in the brace member should be the average for compression and tension load effects in the chord. Based on the previous findings of Ozyurt et al. [20], and confirmed by other researchers, when the brace member is under a compressive load, the joint resistance reduction factor is based on Young's modulus of steel, and when the brace member is under a tensile load, the joint resistance reduction factor is according to the steel yield strength. Therefore, in the case of in-plane bending in the brace member, using the average of the reduction factors for steel Young's modulus and yield stress is reasonable as demonstrated in Fig. 24.

The joint resistance ratios closer to the reduction factor of the yield strength of steel are for β values greater than 0.80. This is because the brace size is almost equal to the chord size, so the chord face failure moves from the top of the chord surface to the side wall. This effect will be further investigated in the following section.

Table 5
Geometric parameters and dimensions for the simulated CHS joints.

Joint Name	d_o (mm)	d_t (mm)	t_o (mm)	t_t (mm)	β (d_t/d_o)	γ ($d_o/2t_o$)
CT90-1, CX90-1, CY45-1, CX45-1, CK45-1	244.5	168.3	8	8	0.69	15.3
CT90-2, CX90-2	244.5	139.7	8	8	0.57	15.3
CT90-3, CX90-3, CK45-2	244.5	114.3	8	8	0.47	15.3
CT90-4, CX90-4	244.5	168.3	12.5	12.5	0.69	9.8
CT90-5, CX90-5	244.5	168.3	10	10	0.69	12.2
CT90-6, CX90-6	244.5	219.1	8	8	0.90	15.3
CT90-7, CX90-7, CK45-3	244.5	244.5	8	8	1.00	15.3
CT90-8, CX90-8	244.5	193.7	8	8	0.79	15.3

Table 6
Geometric parameters and dimensions for the simulated SHS joints.

Joint Name	b_o and h_o (mm)	b_t and h_t (mm)	t_o (mm)	t_t (mm)	β (b_t/b_o)	γ ($b_o/2t_o$)
ST90-1, SX90-1, SY45-1, SX45-1, SK45-1	250	200	8	8	0.80	15.6
ST90-2, SX90-2	250	160	8	8	0.64	15.6
ST90-3, SX90-3, SK45-2	250	120	8	8	0.48	15.6
ST90-4, SX90-4	250	200	12.5	12.5	0.80	10.0
ST90-5, SX90-5	250	200	10	10	0.80	12.5
ST90-6, SX90-6	250	225	8	8	0.90	15.6
ST90-7, SX90-7, SK3-45	250	250	8	8	1.00	15.6

Table 7
Geometric parameters and dimensions for the simulated EHS joints (values of β and γ based on type 2 orientation).

Joint Name	b_o (mm)	h_o (mm)	t_o (mm)	b_t (mm)	h_t (mm)	t_t (mm)	B (b_t/b_o)	Γ ($b_o/2t_o$)
ET90-1, EY45-1, EK45-1, EX90-1	300	150	8	150	75	8	0.50	18.7
ET90-2, EX90-2	250	125	8	150	75	8	0.60	15.6
ET90-3, EX90-3	300	150	10	250	125	10	0.83	15.0
ET90-4, EX90-4	250	125	8	120	60	8	0.48	15.6

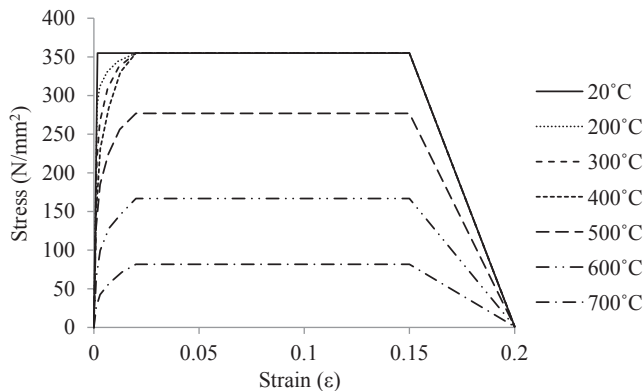


Fig. 20. Stress-strain curves of steel at elevated temperatures.

3.3.2. SHS joints

Fig. 27(a) and (b) present results for SHS T- and Y-, K- and X-joints, respectively, in the same way as for CHS joints in Fig. 24(a) and (b).

The trend in Fig. 27 is the same as in Fig. 24 for CHS joints. This is because the mechanisms affecting SHS joint behaviour at elevated temperatures are the same as for CHS joints.

3.3.3. EHS joints

The same behaviour and conclusions as for CHS and SHS joints can be reached for different types of EHS joints, as confirmed by the results in Fig. 28.

3.4. Welded tubular joints under brace out-of-plane bending moment

There was not any available test result of welded tubular joints under brace out-of-plane bending moment at elevated temperatures. However, the authors used the test results of Nguyen et al. [18] to validate the numerical model for CHS T-joints under brace in-plane bending moment at elevated temperatures and the ambient temperatures tests of Wang et al. [25] to validate the numerical model for out-of-plane bending.

In fact, the trends of joint resistance-temperature relationships for brace in-plane bending also apply to joint resistance-temperature relationships for brace out-of-plane bending, as shown in Figs. 29–31 for CHS, SHS and EHS joints under brace out-of-plane bending respectively. Fig. 32 shows the chord longitudinal stress distribution of a typical joint under out-of-plane bending at elevated temperatures, with half of the chord face in tension and half of the chord face in compression.

3.5. Effects of geometrical parameters on joint resistance

The results have indicated some differences for different joints. This was attributed to effects of different joint geometries. To substantiate this, the effects of non-dimensional parameters of γ and β on joint elevated temperature resistance to ambient temperature resistance ratios are examined. Only CHS T-joints under in-plane bending moment was considered in detail as an example. Fig. 33 assesses the effect of changing γ for CT90-1 ($\gamma = 15.3$), CT90-4 ($\gamma = 9.8$) and CT90-5 ($\gamma = 12.2$). The results confirm that the non-dimensional parameter γ

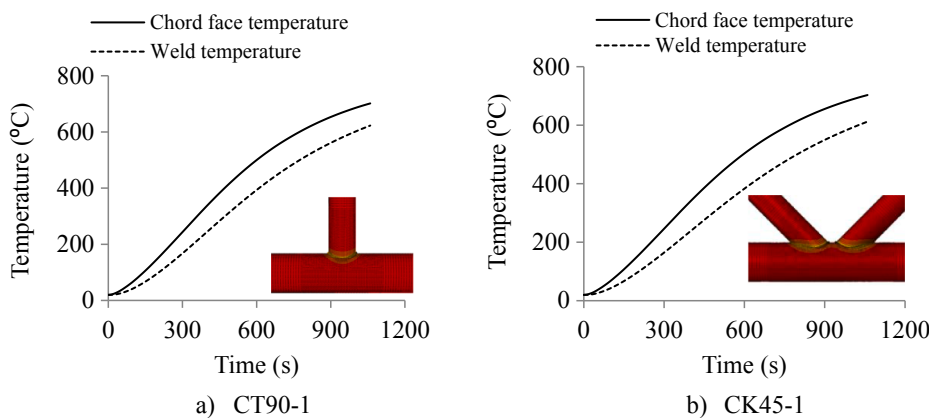


Fig. 21. Comparison of temperature distributions for CT90-1 and CK45-1 joints.

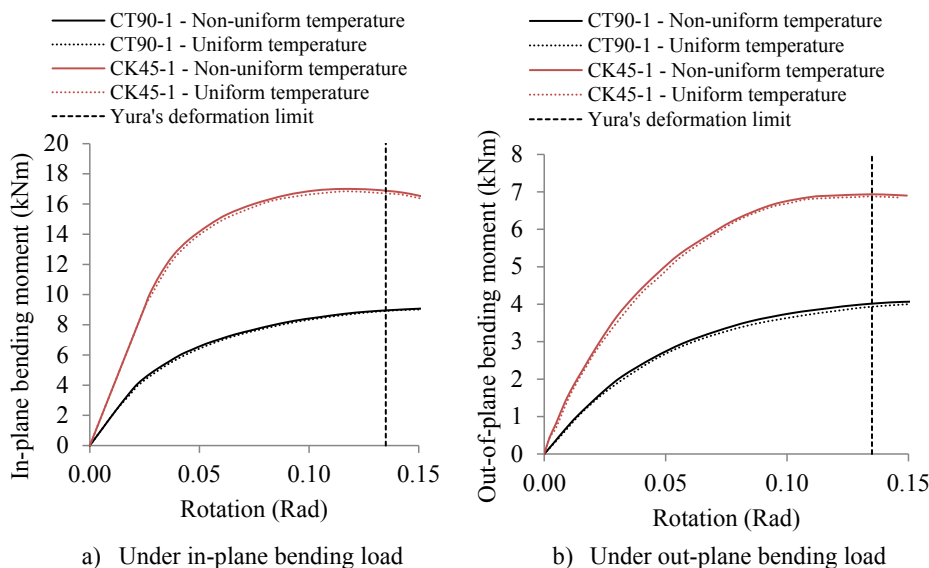


Fig. 22. Comparison of bending moment-rotation curves of CT90-1 and CK45-1 joints between uniform and non-uniform temperature distributions.

has negligible effect on joint resistance ratio.

Fig. 34 presents results for changing the brace to chord diameter ratio (β) for joints CT90-1 ($\beta = 0.69$), CT90-2 ($\beta = 0.57$), CT90-3 ($\beta = 0.47$), CT90-6 ($\beta = 0.90$), CT90-7 ($\beta = 1.00$) and CT90-8 ($\beta = 0.79$). When the brace diameter is much smaller than the chord diameter ($\beta < 0.8$), the joint elevated temperature to ambient temperature resistance ratio is nearly constant at the average value of steel yield strength and Young's modulus reduction factors. With increasing β , the joint resistance ratio increases, almost linearly, until reaching the steel yield strength reduction factor at $\beta = 1.0$.

By introducing this effect of β , the joint elevated temperature resistance to ambient temperature resistance ratio can be more accurately calculated, as shown in Fig. 35. Without including the effect of β , the ratio of calculation results to ABAQUS simulation results, by using the average of steel yield strength and Young's modulus reduction factors at elevated temperatures, have an average value of 1.07 and standard deviation of 0.09. Including the aforementioned β effect in the calculations, the average value is 1.03 and the standard deviation is 0.04.

Structural reliability analyses based on Eurocode 0 [3] have been conducted to quantify the level of reliability of the proposed design

methods. The probabilities of failure (calculated joint resistance ratio less than the simulation resistance ratio) for the proposed design methods including or excluding β effects are 0.079 and 0.076, respectively, corresponding to reliability indices of 1.41 and 1.44, respectively. According to the Eurocode 0 [3], the target reliability index for the most common case (class CC2 structure with a design life of 50 years) is 3.8. Since the target reliability index is greater than the reliability indices of the proposed methods, a safety factor may be introduced to improve the reliability of the proposed methods.

The joint resistance ratios of the numerical simulation result to the proposed design calculation value follow the Gumbel distribution. Defining the characteristic values of the joint resistance ratio (simulation result < design calculation result) as the 5th percentile values, according to Eurocode 0 [3], these are 0.971 and 0.976 respectively for the proposed methods including and excluding the β effect. Based on the Gumbel distribution function given in Table C3 in Eurocode 0 [3], the design values of the corresponding proposed design equations are 0.95 and 0.89, respectively. Therefore, the safety factors (= characteristic/design value) can be calculated as 1.03 and 1.09, respectively.

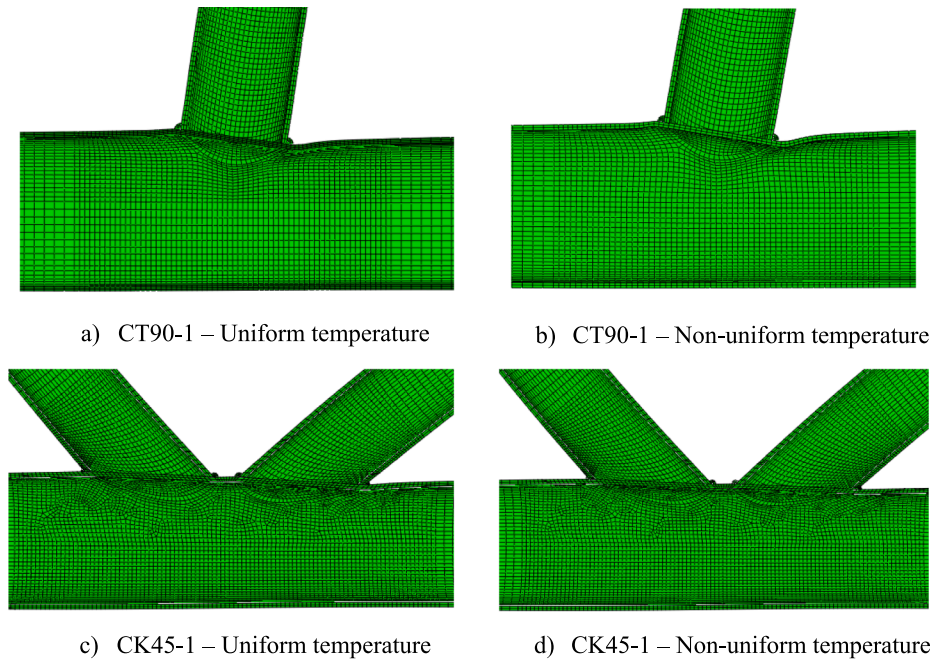


Fig. 23. Comparison of deformed shapes of CT90-1 and CK45-1 joints under a brace in-plane bending moment between uniform and non-uniform temperature distributions.

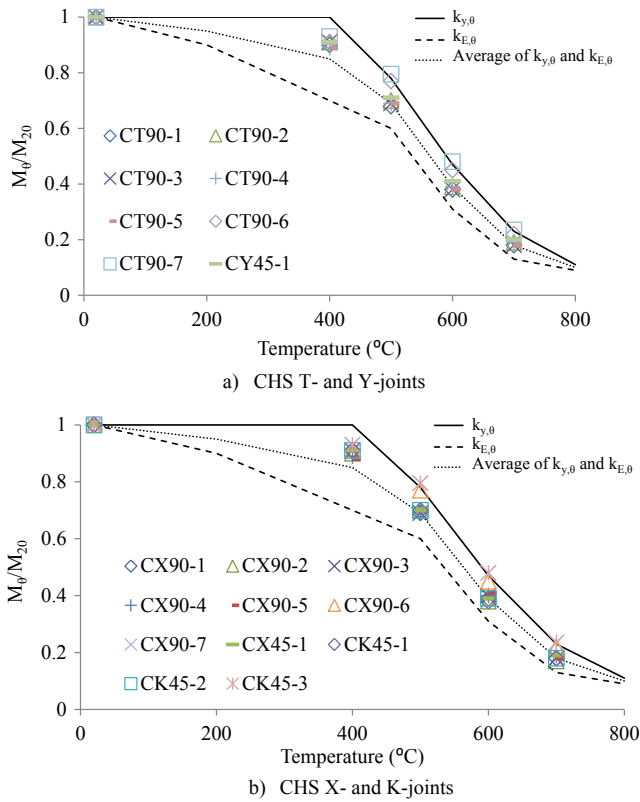


Fig. 24. Variations of resistance of CHS T- and X-joints under in-plane bending.

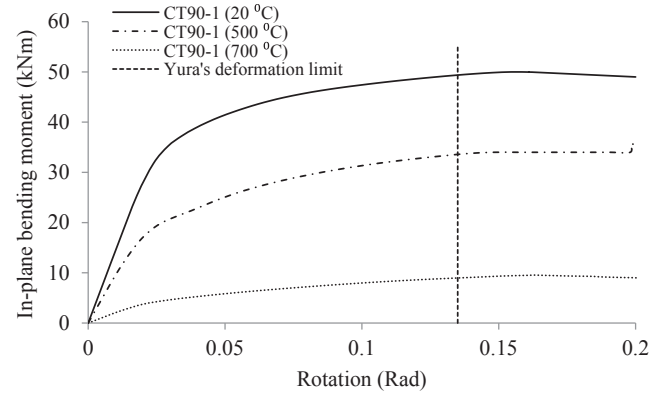


Fig. 25. In-plane bending moment-rotation curves of CT90-1 joints at different temperatures.

4. Conclusions

This paper has presented the results of numerical simulations to investigate chord face behaviour and resistance of welded T-, Y-, K- and X-joints made of SHS, CHS, and EHS at elevated temperatures under brace in-plane or out-of-plane bending moment. The numerical investigation was carried out using the general non-linear FE software ABAQUS, validated against relevant test results. The parametric study covered a comprehensive range of design parameters of brace to chord diameter ratio, width to thickness ratio of the chord, joint type, orientation and section type.

Based on the parametric study results, the following conclusions can be drawn:

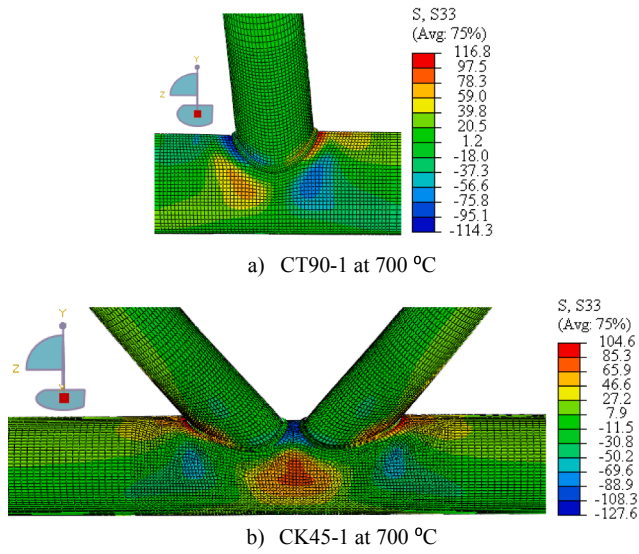


Fig. 26. Stress distributions of selected CHS joints under in-plane loading.

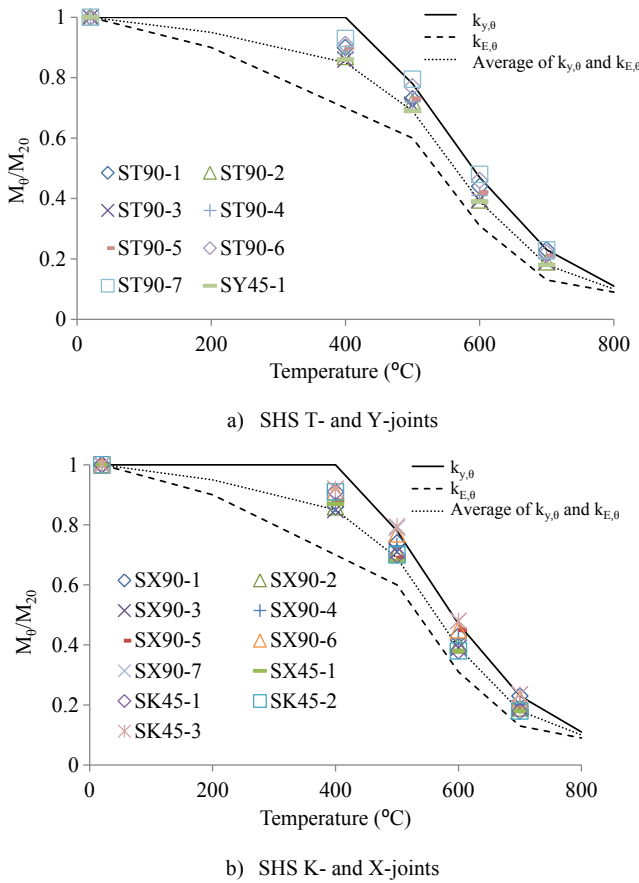


Fig. 27. Variations of resistance of SHS T-, Y-, K- and X-joints under in-plane bending.

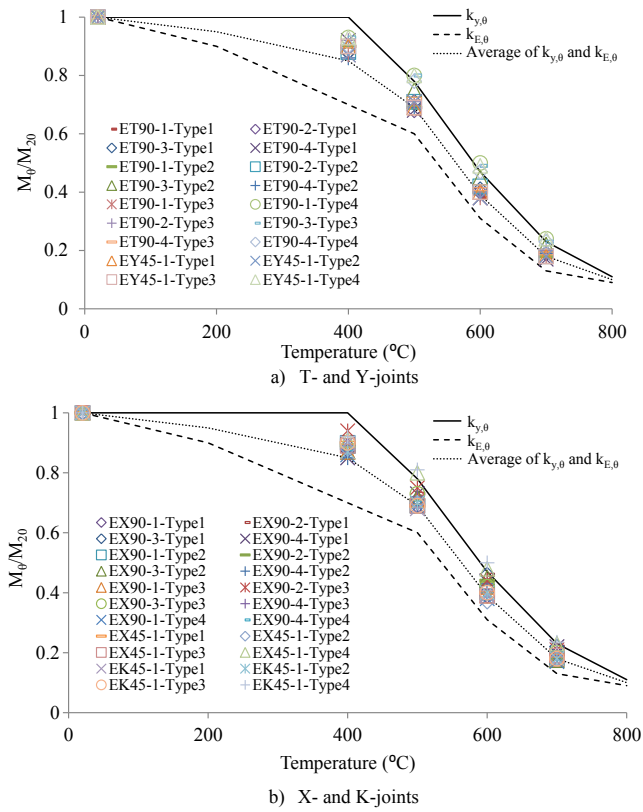


Fig. 28. Variations of resistance of EHS T-, Y-, K- and X-joints under in-plane bending.

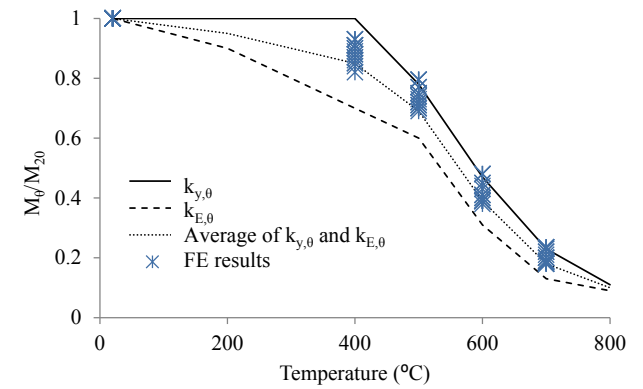


Fig. 29. Variations of resistance of CHS T-, Y-, K- and X-joints under brace out-of-plane bending.

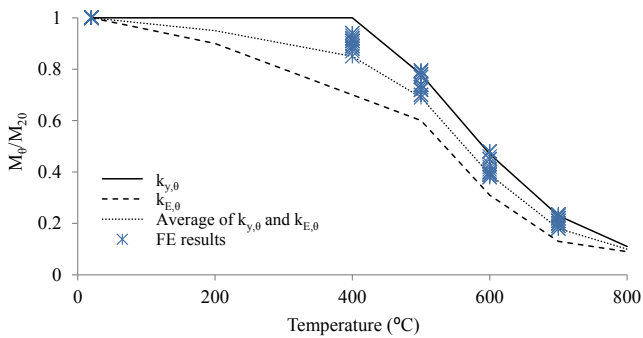


Fig. 30. Variations of resistance of SHS T-, Y-, K- and X-joints under brace out-of-plane bending.

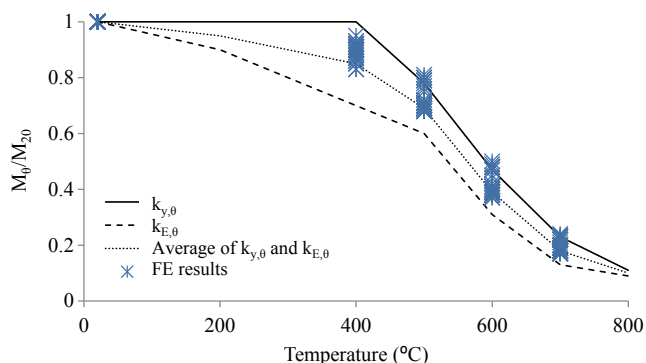


Fig. 31. Variations of resistance of EHS T-, Y-, K- and X-joints under out-of-plane bending.

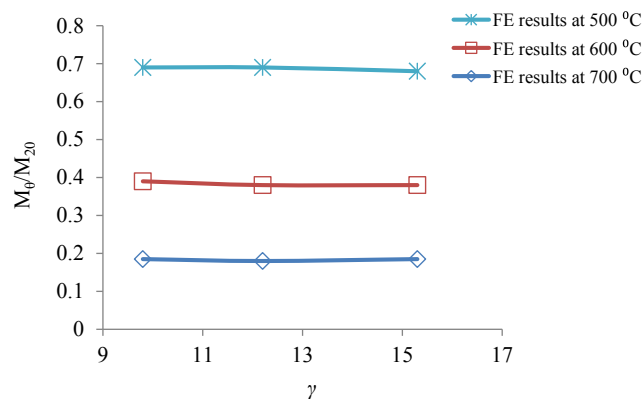


Fig. 33. Effects of γ on joint resistance ratio.

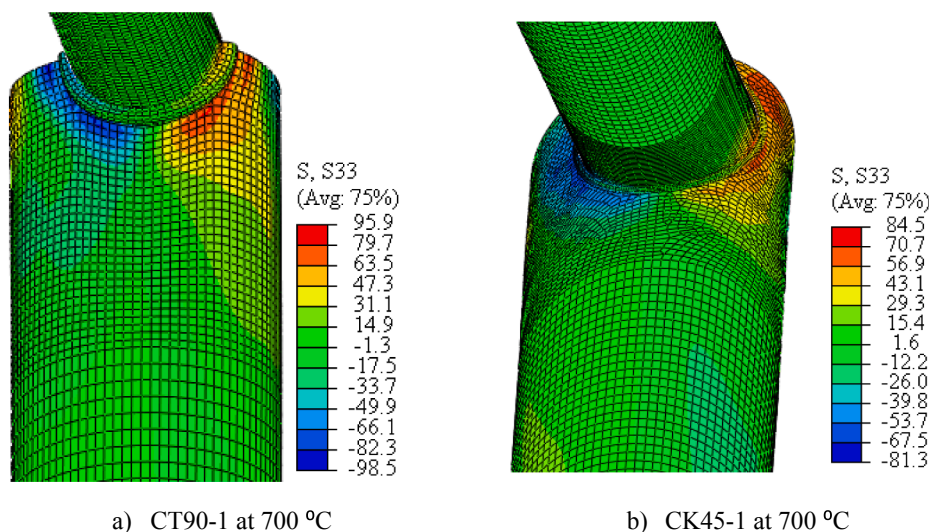


Fig. 32. Stress distributions of selected CHS joints under out-of-plane loading.

- (1) Under both in-plane and out-of-plane bending in the brace, half of the chord face undergoes longitudinal tension and half compression. Therefore, to calculate joint resistance at elevated temperatures, the ambient temperature joint resistance equations can be modified by the average value for joint under brace tension (which results in longitudinal tension in the chord) and for joint under brace compression (which results in longitudinal compression in the chord).
- (2) Previous research studies have established that it would be safe and sufficiently accurate to calculate joint resistances by modifying their ambient temperature resistances by steel yield strength reduction factors for compression and steel Young's modulus reduction factors for tension. Therefore, for both in-plane and out-of-plane bending, the elevated temperature resistance can be safely calculated by modifying the ambient temperature resistance by the average of elevated temperature reduction factors for Young's modulus and yield strength of steel with a safety factor of 1.09.

- (3) When the brace dimension to chord dimension ratio (β) approaches unit, any second order effects in the chord face diminish. Therefore, the ratio of joint resistance at elevated temperature to that at ambient temperature approaches the steel yield strength reduction factor. If it is necessary to improve the accuracy of calculated joint resistance, the elevated temperature joint resistance to ambient temperature joint resistance ratio can be considered to vary linearly, from the average of steel yield strength and Young's modulus reduction factors at $\beta = 0.8$ to steel yield strength reduction factor at $\beta = 1.0$, by including a safety factor of 1.03.
- (4) The conclusions above apply to all joint types and tubular section shapes. They are also independent of other joint geometry factors.
- (5) When an unprotected tubular joint is exposed to fire, the weld region attains lower temperatures. However, for the failure mode of chord face plastification, the effect of this lower weld temperature is very low and can be safely discarded.

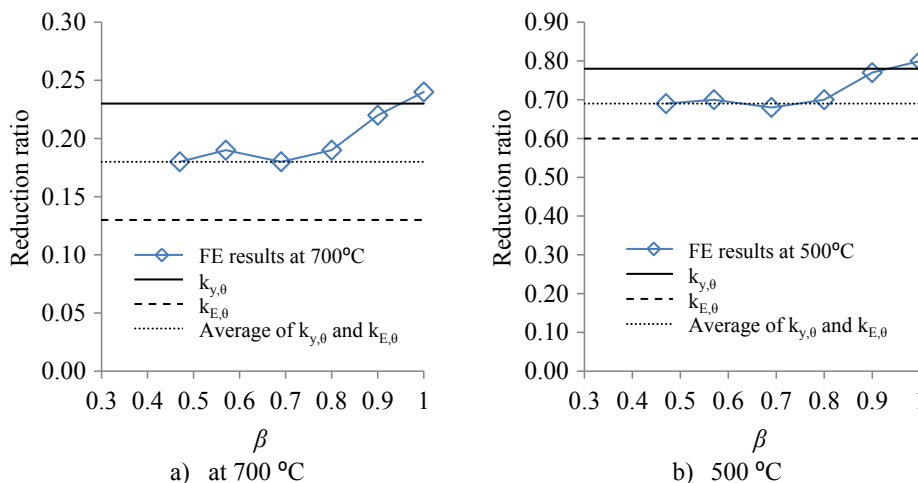


Fig. 34. Effects of β on joint resistance ratios at 500 °C and 700 °C.

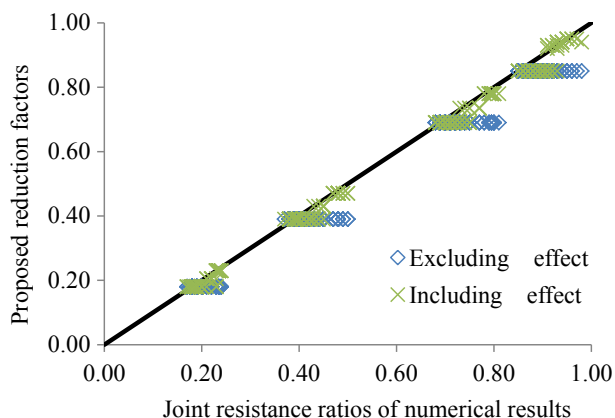


Fig. 35. Comparison for joint resistance ratios between numerical simulation and two different modification factors.

Declaration of Competing Interest

We confirm that there is no conflict of interest for this paper and that we have acknowledged all sources of support.

Acknowledgment

This research is supported by the Scientific and Technological Research Council of Turkey (TUBITAK-BIDEB, 2219 International Post-Doctoral Research Fellowship Programme). The authors would also like to acknowledge partial funding by CIDECT through its project 15U-Joints at high temperatures.

References

[1] Abaqus V. 6.14 documentation. Dassault Systemes Simulia Corporation; 2014.
 [2] Boreis AP, Schmidt RJ. Advanced mechanics of materials. John Wiley and Sons; 2003.
 [3] CEN. Basis of structural design. BS EN 1990:2002 - Eurocode 0. London: British Standards Institution (BSI); 2002.
 [4] CEN. Design of steel structures. In: PART editor. EN 1993-1-8-Design of joints. London: Brussels, Belgium; 2005a.
 [5] CEN. Design of steel structures. In: PART editor. EN 1993-1-2-structural fire design. Brussels, Belgium; 2005b.

[6] CEN. Design of steel structures. In: PART editor. EN 1993-1-1-general rules and rules for building. Brussels, Belgium; 2005c.
 [7] Chen X-X, Chen Y, Chen D-F. Plate reinforced square hollow section X-joints subjected to in-plane moment. J Central South Univ 2015;22:1002–15.
 [8] Chen Y, Chen D. Ultimate capacities formulae of collar and doubler plates reinforced SHS X-joints under in-plane bending. Thin-Walled Struct 2016;99:21–34.
 [9] Cheng C, Shao Y-B, Jie Y. Experimental and numerical study on fire resistance of circular tubular T-joints. J Constr Steel Res 2013;85:24–39.
 [10] Choo Y, Liang J, Lim L. Static strength of elliptical hollow section X-joint under brace compression. Tubular structures-international symposium. 2003. p. 253–8.
 [11] Gao F, Guan X-Q, Zhu H-P, Liu X-N. Fire resistance behaviour of tubular T-joints reinforced with collar plates. J Constr Steel Res 2015;115:106–20.
 [12] Garifullin M, Pajunen S, Mela K, Heinisuo M, Havula J. Initial in-plane rotational stiffness of welded RHS T-joints with axial force in main member. J Constr Steel Res 2017;139:353–62.
 [13] He S, Shao Y-B, Zhang H. Evaluation on fire resistance of tubular K-joints based on critical temperature method. J Constr Steel Res 2015;115:398–406.
 [14] He S, Shao Y-B, Zhang H, Wang Q. Parametric study on performance of circular tubular K-joints at elevated temperature. Fire Saf J 2015;71:174–86.
 [15] Lan X, Huang Y. Structural design of cold-formed stainless steel tubular X-and T-joints at elevated temperatures. Thin-Walled Struct 2016;108:270–9.
 [16] Lan X, Huang Y, Chan T-M, Young B. Static strength of stainless steel K-and N-joints at elevated temperatures. Thin-Walled Struct 2018;122:501–9.
 [17] Nassiraei H, Lotfollahi-Yaghin MA, Ahmadi H, Zhu L. Static strength of doubler plate reinforced tubular T/Y-joints under in-plane bending load. J Constr Steel Res 2017;136:49–64.
 [18] Nguyen M, Fung, TC, Tan K. Structural behavior of CHS T-joints subjected to brace in-plane bending at elevated temperatures. In: GARDNER, editor. Tubular Structures XIV. London, UK; 2012.
 [19] Ozyurt E, Wang Y. Resistance of axially loaded T-and X-joints of elliptical hollow sections at elevated temperatures—a finite element study. Structures 2018:15–31. Elsevier.
 [20] Ozyurt E, Wang Y, Tan K. Elevated temperature resistance of welded tubular joints under axial load in the brace member. Eng Struct 2014;59:574–86.
 [21] Packer JA, Wardenier J, Zhao X-L, Van der vegte GJ, Kurobane Y. Design guide for rectangular hollow section (RHS) joints under predominantly static loading. Verlag TUV Rheinland, Germany: CIDECT; 2009.
 [22] Shao Y-B, Zhao H, Yang D. Discussion on two methods for determining static strength of tubular T-joints at elevated temperature. Adv Struct Eng 2017;20:704–21.
 [23] Shao Y-B, Zheng Y, Zhao H, Yang D. Performance of tubular T-joints at elevated temperature by considering effect of chord compressive stress. Thin-Walled Struct 2016;98:533–46.
 [24] Van der vegte G, Makino Y. Further research on chord length and boundary conditions of CHS T-and X-joints. Adv Steel Constr 2010;6:879–90.
 [25] Wang C, Chen Y, Chen X, Chen D. Experimental and numerical research on out-of-plane flexural property of plates reinforced SHS X-joints. Thin-Walled Struct 2015;94:466–77.
 [26] Wardenier J, Kurobane Y, Packer JA, Van der vegte GJ, Zhao X-L. Design guide for circular hollow section (CHS) joints under predominantly static loading. Cidect; 2008.
 [27] Yura JA, Zettlemoyer NA, Edwards IF. Ultimate capacity equations for tubular joints. In: Offshore technology conference; 1980.